Modulation of Vortex Induced Crosswind Forces on a Square Cylinder During Accelerating Flow

M.S. Mason[1] and T. Yang[1]

[1]School of Civil Engineering
University of Queensland, Queensland 4072, Australia

Abstract

Severe wind storms are transient phenomena that are often characterised by periods of rapidly accelerating wind speed. The impact of this flow acceleration on structural loading is currently unknown but is believed to play a role in instigating failure during these events. This paper describes a series of wind tunnel experiments undertaken to investigate how crosswind forces on a two-dimensional square cylinder varied during a period of rapid acceleration. Results show that when flow acceleration began from an initial quiescent state, both the amplitude and frequency of force coefficient fluctuations exceeded what was recorded during steady flow tests at similar Reynolds Numbers. However, when flow was accelerated from a non-zero initial state, steady results were replicated for both amplitude and frequency throughout much of the acceleration period. The only exception to this was a small increase in fluctuation amplitude near the end of the period of flow acceleration. This finding has implications for structural design, but requires further research to validate.

Introduction

Wind gusts that damage structures are often associated with extreme atmospheric events such as tornadoes, tropical cyclones or thunderstorm outflows. These events are highly transient and, at their peak, only load structures for a short period of time, i.e. seconds or minutes. Despite this, wind-resistant design practice is based on the assumption that all wind and its resulting structural loads are temporally stationary. This leads to a potential mismatch between the loads structures are being designed to withstand and those they actually see during strong wind events.

Continued damage during strong wind storms has brought the stationarity simplification into question and researchers have begun exploring the potential consequences of this assumption [6]. For example, [3,5,7] examined wind loads on model structures in unsteady impinging jet facilities, simulating the loading profiles experienced during downburst-like wind events. Similarly, [2,8] investigated loading profiles during the passage of simulated tornado events in small-scale simulators. In these experiments highly complex flow fields where generated and the local wind speed, wind direction and boundary layer that loaded a given structure all changed rapidly with time. For each it was concluded that wind loads differed from those expected during traditional stationary boundary layer winds, but did not explain why these differences existed. The reason for this is that the constituent influences, i.e. transience of wind speed, direction and boundary layer structure, were not studied in isolation and therefore much of the physical reasoning for differences was unclear.

This paper attempts to isolate and explore one of the potential factors that influence wind loading during strong wind storms; its transient wind speed. By investigating this factor alone its resultant influence on loading can be systematically studied and greater fundamental understanding of its importance built. To do this, a series of experiments were carried out in an actively controlled wind tunnel, where wind loads on a two-dimensional square cylinder were measured during rapidly accelerating flow. In this paper we focus on the time dependent crosswind lift forces applied to the cylinder as previous research suggests these may be amplified during periods of acceleration [9,10]. Results are compared with steady flow tests and relative differences identified.

Wind tunnel setup and procedure

All experiments were conducted in the University of Queensland Eiffel-style active gust wind tunnel (760 mm x 760 mm x 2360 mm test section). Flow is driven by a vane-axial fan, which can accelerate winds at rates up to 11 ms^{-2}. When run at a constant frequency, a uniform velocity field exists across the tunnel with a turbulence intensity below 0.5%.

Experiments were subject to flow acceleration from an initial steady velocity, U_s, to a target velocity, U_t, over a short duration. U_t was 25.5 ms^{-1} for all experiments and U_s was either 0 ms^{-1}, 8.4 ms^{-1} or 17.0 ms^{-1}, the latter two corresponding to $U_t/3$ and $2U_t/3$. The characteristic tunnel acceleration, a_c, remained constant for each test at the maximum rate of approximately 11 ms^{-2}. Thirty repeat tests were run for each initial velocity case so test-to-test variability could be assessed and ensemble data generated. Figure 1 shows the mean wind speed time history for the accelerating portion of the three cases considered. Wind speed is shown normalised to a time-dependent Reynolds Number, $Re = u(t)D/v$, where u(t) is the reference wind speed, D is the model side length (60 mm), v the kinematic viscosity of air and t is time.
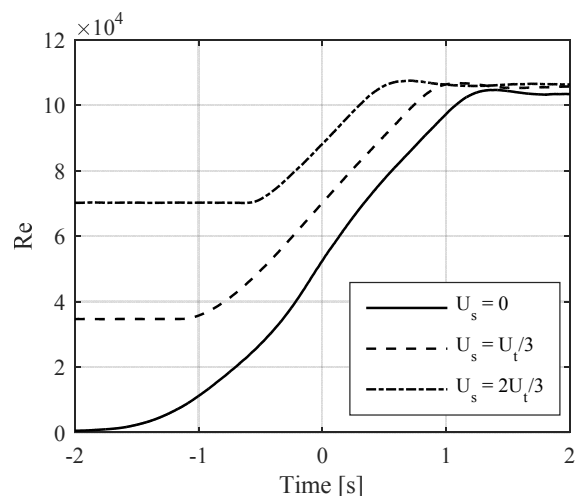

Figure 1. Ensemble mean of instantaneous Reynolds Number time histories for the three acceleration cases.

Surface pressures were circumferentially measured around the centreline of the square cylinder, which presented a blockage ratio of 7.5%, Figure 2. Pressure taps were connected to a Scanivalve

ZOC-33 pressure scanning system through 1.5 m of 1.5 mm PVC tubing. Static pressures were measured on the floor of the tunnel vertically aligned with the front of the model using the same tubing arrangement. A hotwire was positioned 100 mm from the top of the tunnel and also aligned with the leading face of the model. Pressure and velocity data were acquired using different data logging systems but were aligned by assigning $t = 0$ to the first exceedance of $(U_t-U_s)/2$ and the corresponding square root of the ratio of this velocity to U_t multiplied by the target pressure measured at the centre tap of the windward face. Circular end plates were attached to the model 300 mm either side of the centreline pressure taps.

Pressure data was acquired at 600 Hz and digitally corrected for phase and amplitude shifts introduced by the transducer and tubing setup. Reference velocities were also acquired at 600 Hz. Using these data lift force coefficient, $C_{L,t}$, time histories were generated by integrating pressures over the top and bottom faces of the model, using

$$C_{L,t} = \frac{\sum\left[(p_t(t) - p_s(\tilde{t})) \cdot \delta d\right]}{\rho u(\tilde{t})^2 D/2} \tag{1}$$

where $p_t(t)$ is the instantaneous tap pressure, $p_s(\tilde{t})$ a smoothed floor tap static pressure, δd the tributary circumferential length of each tap, ρ the density of air and $u(\tilde{t})$ the smoothed reference velocity. The presence of a time dependent reference velocity in the denominator of Equation 1 means that if the body aerodynamics remain constant throughout flow acceleration, the lift coefficient should also be constant over this period.
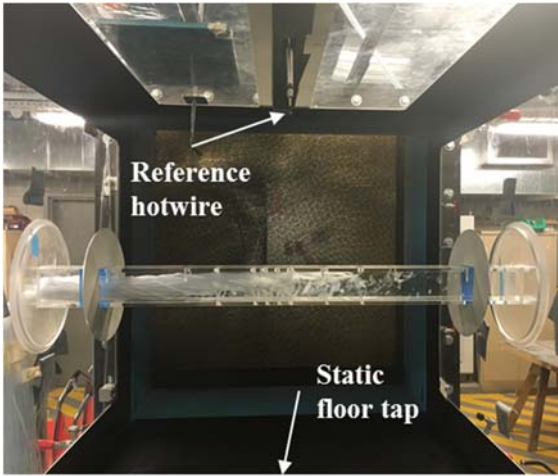

Figure 2. Wind tunnel setup.

Results and discussion

Lift coefficient time histories

Figure 3 shows lift coefficient time histories for a single run of each of the three initial velocity test cases. Plot also are the 10% and 90% bounds of the distribution of negative and positive peaks, respectively, for the thirty ensemble members of each case. The period of accelerating flow is indicated by dashed blue lines.

The (predominantly) symmetric oscillatory nature of the lift coefficient signal is evident for all runs. Qualitatively, two observations are made; 1) except for an initial period of large amplitude, high frequency fluctuations for the $U_s = 0$ case, the frequency of oscillations increases as flow accelerates from U_s to U_t. 2) The amplitude of oscillations (in an ensemble sense) remains reasonably constant for the $U_s = U_t/3$ and $2U_t/3$ cases, but undergoes a period of growth following the aforementioned large amplitude, high frequency fluctuations for the $U_s = 0$ case.

Both points can be conceptually understood by considering the physical process of vortex shedding. For point 1, the non-dimensional Strouhal Number ($St = fD/u$) typically used to quantify shedding frequency, f, shows that for St to remain constant a linear relationship between wind speed and frequency must exist. This appears to qualitatively hold for each case, except in the early stages of $U_s = 0$ tests where we hypothesise that low wind speeds and a developing wake region have led to high frequency chaotic fluctuations in $C_{L,t}$. For point 2, while the ensemble amplitude bounds do show consistency in the latter two cases, each individual run displays variability with time (i.e. peaks do not remain constant from one cycle to the next). This observation is characteristic of vortex shedding in low turbulence flows [1]. Vortex shedding can also explain the growth of $C_{L,t}$ during the period -1 s < t < 0 s in the $U_s = 0$ case. Prior to this time, we hypothesise, no systematic shedding exists and it is during this period that discrete vortices develop and are subsequently shed from the body. For this to occur the wake must transition from still air to one dominated by coupled vortices, therefore a development phase should be expected and is observed.

(a) $U_s = 0$
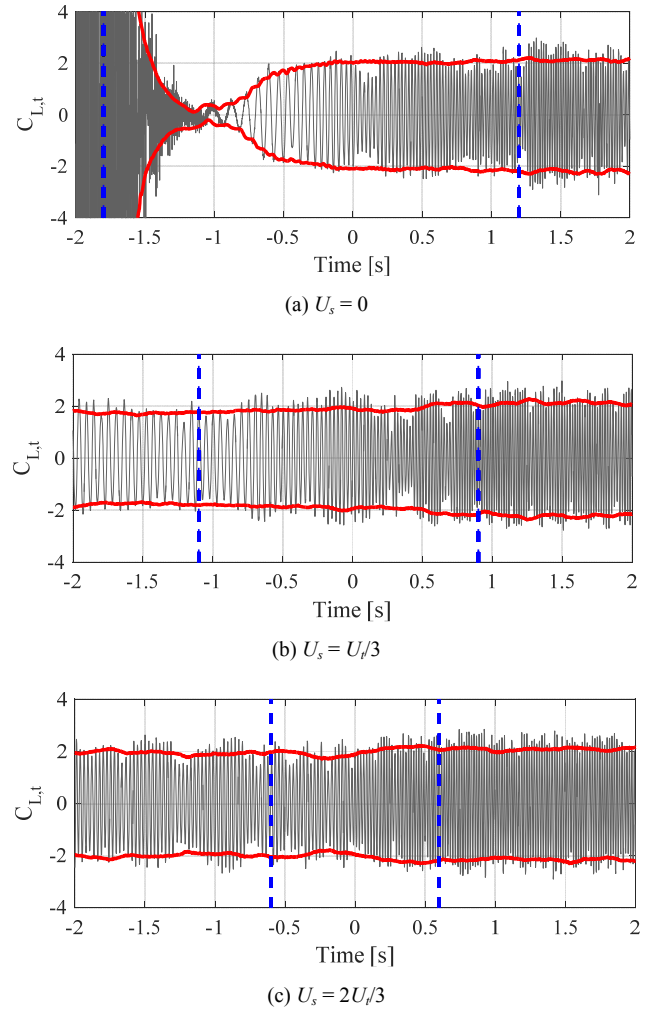

(b) $U_s = U_t/3$

(c) $U_s = 2U_t/3$

Figure 3. Lift force coefficient time histories for a single run of each of the three initial velocity cases. Dashed blue lines indicate the period of acceleration and the solid red lines the 10% and 90% peak bounds for all thirty runs of each test case.

One feature that is absent from all results is any significant overshooting in lift force amplitude associated with the period of flow acceleration. Such a phenomenon was reported by [10] for lift and drag on a yawed elliptic cylinder and by [9] for drag on a square cylinder when loaded by a similar accelerating wind field to that tested here (the latter did not report lift results). In some

cases, [10] showed this overshoot to be 5-6 times the mean lift force on their cylinder. The presence of such an overshoot would have significant ramifications for designing wind-resistant structures. Possible reasons for the discrepancy between findings of [9-11] and those presented here, as well as a more qualitative analysis of data presented in Figure 3, are explored further in the following sections.

Amplitude analysis

To quantitatively analyse the amplitude of lift force coefficient oscillations, both positive, $\hat{C}_{L,t}$, and negative, $\check{C}_{L,t}$, peaks were identified and extracted for each run. The time of each peak was identified and an associated wind speed determined. Using these data an instantaneous Reynold Number, Re, based on $u(\tilde{t})$, could be assigned to each peak. Discretising these data into bins, amplitude information for each of the thirty runs for each case could be aggregated and mean amplitude information calculated. This has been done for both positive and negative peaks but given the similarity of these data absolute peak amplitudes, $\overline{|\hat{C}_{L,t}|}$, are used for the subsequent analysis to maximise data utilised.

Figure 4 shows the relationship between the ensemble mean of peak lift coefficient amplitudes, $\overline{|\hat{C}_{L,t}|}$, and Re for the three test cases. Data is shown for the period of acceleration only, as indicated in Figure 3 (i.e. between the blue dashed lines), except for the $U_s = 0$ case where only data for t > -1.2 s shown. Plot also is the mean coefficient amplitude measured from 180 seconds of steady flow data with the tunnel set to U_t/3, $2U_t$/3 and U_t.
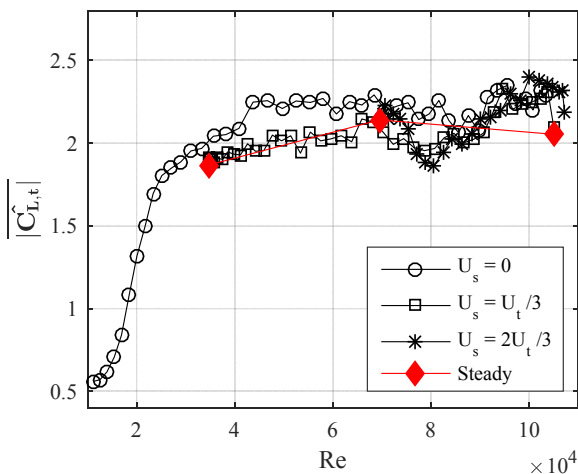

Figure 4. Ensemble mean of peak lift coefficients for each of the three initial velocity cases.

Inspecting first steady flow amplitudes, it is evident that some variability exists throughout the Re range tested. While only on the order of 10%, this observation highlights that flow is being accelerated through a range where peak lift coefficient amplitudes have some variability.

For $U_s = 0$ Figure 4 clearly shows the period of amplitude growth as flow accelerates through the low Re range. The amplitude reaches a constant value of approximately 2.25 for Re > 4×10^4, with little variability until near the end of the flow acceleration period. Of note is that following the initial growth period, peak amplitudes remain between 5% and 10% higher than for steady flow and similarly remain greater than measured for the other initial velocity cases.

Both U_t/3 and $2U_t$/3 cases begin their periods of acceleration with a mean ensemble amplitude equal to that of the steady flow with an equivalent U_s. The $U_s = U_t$/3 amplitude increases from 1.9 to approximately 2.2 while accelerating to $2U_t$/3, which closely approximates the steady flow magnitude at this Re. Following this

point, the amplitude drops back to around 2 before then increasing back to 2.2 in the latter part of the acceleration phase. The $U_s = 2U_t$/3 case follows the U_t/3 trend closely, with the drop and gradual rise in amplitude again observed. It is unclear whether this behaviour is reflected in steady flow amplitudes over this range, and further testing is required to determine whether it is flow acceleration or simply a Re dependence that is being observed.

While the qualitative analysis of Figure 3 noted that no obvious overshoot in lift coefficient amplitude was observed, Figure 4 does seem to suggest all cases display an amplitude approximately 10% higher than for steady flow tests at the end of the acceleration period. Some indication of magnitudes dropping back to the steady flow level are present, but a more thorough analysis of both steady flow amplitudes and those in the immediate period following U_t being reached are required to draw any firm conclusions.

When comparing these observations with those of [9,10], even if the amplitude increase over steady flow tests discussed in the previous paragraph is proven, the magnitude observed here is significantly lower. This occurs for two reasons. Firstly, flow acceleration in the current tests is less than many of [9,10] tests, which generated the largest overshoots. Since such overshoots are largely driven by acceleration-dependent inertial forces introduced by the unsteadiness of flow, the smaller the acceleration the smaller the overshoot expected. Secondly, because inertial forces are not, to a first order, dependent on Re [4], but traditional lift and drag forces are, as Re increases the relative magnitude of body to inertial forces increase. Given current experiments utilise a much higher U_t than previously used, the contribution of any inertial forces to the total observed force (and its resultant overshooting) is substantially less.

In summary, further steady flow tests are required to ascertain conclusively whether any increase in amplitude has occurred during flow acceleration when beginning from a non-zero initial velocity. When starting from zero though, a period of wake development and subsequent stabilisation occurs, where during the latter period peak lift coefficient amplitudes exceed steady flow experiments by approximately 10% over much of the Re range. What is clear though, is that for the Re tested here overshooting of lift coefficients is significantly less than observed by previous authors at smaller target Re.

Frequency analysis

To quantitatively assess the frequency of lift coefficient oscillations, times associated with extracted $\hat{C}_{L,t}$ and $\check{C}_{L,t}$ series were identified. Discretely measuring the time period between successive peaks, a cycle period and subsequent frequency could be calculated. Averaging the reference wind speed at successive peaks then allowed the relationship between instantaneous Re and non-dimensional frequency, St, to be ascertained.

Figure 5 (a) shows an example of frequency data extracted using the discrete measurement process outlined above for the time history shown in Figure 3 (a) (excluding the initial low Re component of the acceleration period). By measuring frequency in this manner, it is evident that only a limited set of discrete frequencies, each associated with the finite number of time steps ($\Delta t = 1/600$ s) between peaks, are possible. Therefore, it appears that data is potentially under-sampled for making such direct frequency measurements, and an alternate method is required. For this a continuous wavelet transform with Morlet filter has been implemented so a more continuous measure of frequency throughout the period of acceleration is provided. Figure 5 (b) shows the frequency content within the signal shown in Figure 3 (a) with the time dependent maxima extracted and plot with the discrete frequency measurements in Figure 5 (a). A smoother representation of the time dependent frequency is shown, with wavelet based frequency estimates used for subsequent analysis.
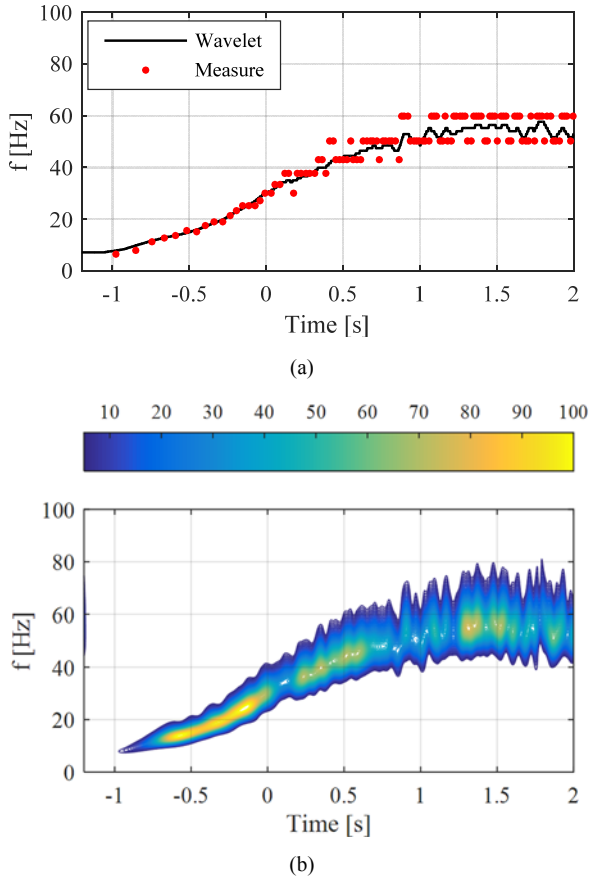
(a)

(b)

Figure 5. (a) Time dependent frequency content for the lift coefficient time history shown in Figure 3 (a) extracted using discrete measurements and the maxima of a continuous wavelet transform (CWT). (b) Frequency component analysis of the lift coefficient time history shown in Figure 3(a) using the CWT.
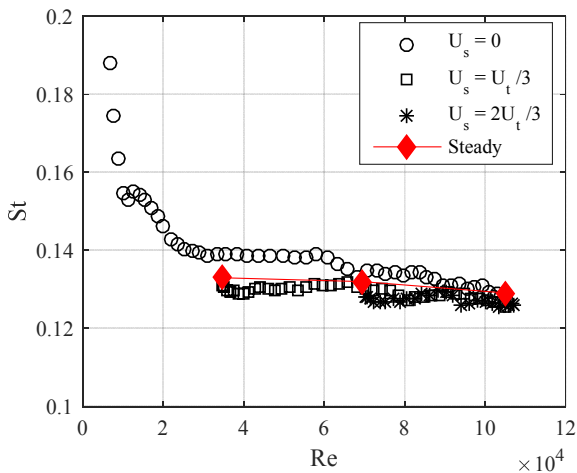

Figure 6. Ensemble mean instantaneous Strouhal Number for each case plot against instantaneous Reynold Number.

Figure 6 shows the relationship between wavelet derived Strouhal Numbers, St, and instantaneous flow Re. As in Figure 4 the ensemble mean for each initial velocity case is shown for the period of flow acceleration with a limited set of steady flow results also included.

Steady flow St values show a small decreasing dependency on Re. This is reflected in both the $U_t/3$ and $2U_t/3$ cases, where a good replication of steady flow frequencies is seen throughout the entire acceleration period. For the $U_s = 0$ case, however, larger St values

are observed for low instantaneous Re, which don't collapse onto other test results until the end of the flow acceleration period. It is therefore evident that for cases where $U_s = 0$, both the amplitude and frequency of lift coefficient fluctuations are greater than for $U_s \neq 0$ cases over much of the period of acceleration, but do collapse near the end of this period.

Conclusions

Experiments were carried out in an actively controlled wind tunnel to determine the unsteady lift force coefficients on a two-dimensional square cylinder during a period of accelerating flow. Based on limited comparisons with steady state tests, flow acceleration is found to have little influence on both the amplitude and frequency of fluctuating lift force coefficients when the initial flow velocity is greater than zero. This may break down near the end of acceleration phase though, where amplitudes 10% greater than those observed in steady state tests look to be occurring. For tests where the initial flow velocity was zero, periods of wake development and stabilisation mean both normalised amplitude and frequency magnitudes are greater than for steady state tests, but these collapse onto the other unsteady results near the end of the acceleration period. Future tests using different acceleration rates and body shapes will more broadly assess these initial findings and their potential implications for wind engineering.

Acknowledgments

References

[1] Carassale, L., Freda, A. & Marre-Brunenghi, M., Experimental investigation on the aerodynamic behaviour of square cylinders with rounded corners, *J. Fluids & Struct.* **44**, 2014, 195-204.

[2] Haan, F., Balaramudu, V. & Sarkar, P., Tornado-induced wind loads on a low-rise building, *J. Struct. Eng.* **136**, 2010, 106-116.

[3] Jesson, M., Sterling, M., Letchford, C. & Haines, M., Aerodynamic forces on generic buildings subject to transient, downburst-type winds. *J. Wind. Eng.*, **137**, 2015, 58-68.

[4] Keulegan, G. & Carpenter, L., Forces on cylinders and plates in an oscillating fluid, *J. Res. Nat. B. Stand.*, **60**, 1958, 423-440.

[5] Letchford, C. & Chay, M., Pressure distributions on a cube in a simulated thunderstorm downburst. Part B: moving downburst observations, *J. Wind. Eng.*, **90**, 2002, 733-753.

[6] Letchford, C., Mans, C. & Chay, M., Thunderstorms—their importance in wind engineering (a case for the next generation wind tunnel), *J. Wind. Eng.*, **90**, 2002, 1415-1433.

[7] Mason, M., James, D., Letchford, C., Wind pressure measurements on a cube subjected to pulsed impinging jet flow. *Wind Struct.* **12**, 2009, 77-88.

[8] Mishra, A., James, D., Letchford, C., Physical simulation of a single-celled tornado-like vortex, Part B: Wind loading on a cubical model, *J. Wind. Eng.*, **96**, 2008, 1258-1273.

[9] Shirato, H., Maeta, K., Kato, Y. & Takasugi, Y., Transient drag force on 2-D bluff bodies under gusty wind conditions, in *7th APCWE*, Taipei, 2009.

[10] Takeuchi, T., Maeda, J., Otsubo, K. & Shuto, Y., Unsteady wind force on an elliptic cylinder subjected to a short-rise-time gust from steady flow, in *7th BBAA*, Shanghai, 2012, 621-630.